https://doi.org/10.5194/acp-2020-395
Preprint. Discussion started: 13 May 2020

Atmospheric Chemistry and Physics Discussions

Characteristics of sub-10 nm particle emissions from in-use commercial aircraft observed at Narita International Airport

Nobuyuki Takegawa[1], Yoshiko Murashima[2], Akihiro Fushimi[3], Kentaro Misawa[1], Yuji Fujitani[3], Katsumi Saitoh[3,4], and Hiromu Sakurai[2]

[1]Department of Chemistry, Graduate School of Science, Tokyo Metropolitan University, Hachioji, Tokyo 192-0397, Japan.
[2]National Institute of Advanced Industrial Science and Technology, Tsukuba, Ibaraki 305-8563, Japan.
[3]National Institute for Environmental Studies, Tsukuba, Ibaraki 305-8506, Japan.
[4]Environmental Science Analysis and Research Laboratory, Hachimantai, Iwate 028-7302, Japan.

Correspondence to: Nobuyuki Takegawa (takegawa@tmu.ac.jp)

Abstract. Civil aviation is undergoing rapid growth as a result of global economic development. Characterizing ultrafine particle emissions from jet aircraft equipped with turbofan engines, which are commonly used in civil aviation, is an important issue for the assessment of the impacts of aviation on climate and on human health. Previous studies have reported that particle number emissions from jet aircraft are dominated by volatile particles (mainly sulphate and organics) with mode diameters of 10–20 nm and that non-volatile particles (mainly soot) exhibit mode diameters of ~20–60 nm, depending on the engine types and thrust conditions. However, there are significant uncertainties in measuring particles with diameters smaller than ~10 nm, especially when fresh aircraft exhaust plumes are measured near the emission sources. We conducted field observations of aerosols and carbon dioxide (CO_2) near a runway of Narita International Airport, Japan, in February 2018, with specific focuses on the contributions of sub-10 nm size ranges to total and non-volatile particles. Spiked increases in particle number concentrations and CO_2 were observed to be associated with wind directions from the runway, which can be attributed to diluted aircraft exhaust plumes. We estimated the particle number emission indices (EIs) for discrete take-off plumes. The median total particle number EI with diameters larger than 2.5 nm was ~60 times greater than the median non-volatile particle number EI with diameters larger than 10 nm for take-off plumes. This value can be interpreted as the difference between total particle number emissions under real-world conditions and non-volatile particle number emissions regulated by standard engine tests. More than half of particle numbers in the plumes were found in the size range smaller than ~10 nm on average for both total and non-volatile particles. The mode diameters of the size distributions of particle number EIs were found to be smaller than ~10 nm in most cases, and the peak EI values were larger than those previously reported under real-world operating conditions. This study provides new insights into the significance of sub-10 nm particles in aircraft exhaust plumes under real-world conditions, which is important in understanding aviation impacts on human health and also in developing aviation emission inventories for regional and global models.

https://doi.org/10.5194/acp-2020-395
Preprint. Discussion started: 13 May 2020

Atmospheric Chemistry and Physics Discussions

1 Introduction

Civil aviation is rapidly growing as a result of global economic development. Consequently, the environmental impact of aircraft emissions has been recognized as an important issue (ICAO, 2017; Masiol and Harrison, 2014; Stacey, 2019). A unique aspect of aircraft emissions is that they can supply gaseous and particulate matter directly to the global atmosphere without any wet removal processes. From the viewpoint of impacts on climate, the primary importance of aviation-produced aerosol particles is that they can significantly affect number concentrations of Aitken-mode particles and, potentially, the formation of clouds in the upper troposphere (Lee et al., 2010; Righi et al., 2016). Specifically, soot or black carbon (BC) particles emitted from aircraft at their cruising altitudes could have a key role in the formation of contrail cirrus clouds (Kärcher and Voigt, 2017; Kärcher, 2018). From the viewpoint of risk to human health, ultrafine particles (UFPs; diameters of <100 nm) emitted from aircraft have become a public concern, especially near airports (Masiol and Harrison, 2014; Stacey, 2019). UFPs can efficiently deposit onto nasal, tracheobronchial, and alveolar regions in the human respiratory system, and uptake and translocation (physical clearance) of solid UFPs such as soot into the blood and lymph circulation could be an important pathway (Oberdörster et al., 2005). Moreover, the surface reactivity of aviation-induced soot particles may increase with decreasing particle size (Jonsdottir et al., 2019).

A number of experiments have been performed at engine-test facilities and under real-world conditions to investigate gaseous and particulate emissions from aircraft equipped with turbofan engines, which are commonly used in civil aviation (e.g., Hagen et al., 1998; Petzold et al., 1999, 2005; Kärcher et al., 2000; Brock et al., 2000; Herndon et al., 2008; Westerdahl et al., 2008; Onasch et al., 2009; Kinsey, 2009; Timko et al., 2010; Lobo et al., 2015a, 2015b; Moore et al., 2017a, 2017b; Kinsey et al., 2019; Yu et al., 2017, 2019; Durdina et al., 2019). The key findings from the previous studies include the following two points. First, significant evolution of volatile particles with diameters smaller than ~10 nm can take place during plume expansion, depending on the sulfur content of the fuel and the age of the plume (Petzold et al., 1999, 2005; Kärcher et al., 2000; Brock et al., 2000, Onasch et al., 2009; Timko et al., 2010). Secondly, non-volatile particles, which are assumed to be equivalent to soot or BC particles, primarily have sizes in the range larger than ~10 nm (geometric mean diameter (GMD) of ~20–50 nm) under various operating conditions, with largest GMDs under ~100% engine-thrust conditions (Petzold et al., 1999; Lobo et al., 2015a, 2015b; Durdina et al., 2019). Zhang et al. (2019) recently proposed a global-scale aviation emission inventory for BC particles by integrating existing datasets of non-volatile particle emission indices (EIs).

Alongside these scientific studies, the International Civil Aviation Organization (ICAO) has authorized a new regulatory standard for mass and number emissions of particles emitted from aircraft engines (ICAO, 2017). In the method for measuring non-volatile particle number concentrations described in the Aerospace Recommended Practice 6320, issued by the Society of Automotive Engineers (SAE-ARP6320) (SAE, 2018), the number concentrations of aerosol particles with diameters larger than 10 nm are measured downstream of a volatile particle remover (VPR) heated to 350°C. Some of the previous studies mentioned above employed sampling methods equivalent to SAE-ARP6320 (Lobo et al., 2015a).

https://doi.org/10.5194/acp-2020-395
Preprint. Discussion started: 13 May 2020


Atmospheric Chemistry and Physics Discussions

A common issue in measuring UFPs in the previous scientific studies and in the regulatory standard is that there are significant losses of particles in the sampling tubes and/or the VPR when fresh aircraft exhaust plumes are sampled directly behind jet engines (Kinsey, 2009; Lobo et al., 2015a, 2015b; Durdina et al., 2019). Although corrections for particle losses have been extensively evaluated and are carefully considered for quantifying particle number concentrations, the absolute values of the correction factors and relative errors associated with the correction tend to be larger for smaller particles (Kinsey, 2009; Lobo et al., 2015a, 2015b; Durdina et al., 2019). Furthermore, the large uncertainty in measuring particle number size distributions with diameters smaller than ~20 nm by using mobility size spectrometers is also of great concern (Wiedensohler et al., 2012). These technical issues should be properly considered for better characterization of aircraft exhaust particles.

We conducted field measurements of UFPs near a runway of Narita International Airport (NRT), Japan, in February 26, 2018 (Fushimi et al., 2019). We used multiple instruments for the measurements of particle number concentrations and size distributions and carefully investigated the performance and consistency of these instruments. The purpose of the present study is to investigate the emission characteristics of sub-10 nm particles from commercial aircraft operating under real-world conditions.

2 Experimental

2.1 Field observations

The field measurements were performed in two containers placed at an observation point ~180 m from the centreline of runway A (~140 m from the edge of the runway) of NRT between February 5 and February 26, 2018 (Fushimi et al., 2019). Fig. 1 shows an approximate layout of NRT with the location of the observation point. The aerosol instruments used for the field measurements consisted of an ultrafine condensation particle counter (UCPC: Model 3776; TSI, Inc., Shoreview, MN, USA; d_{50} = 2.5 nm), a condensation particle counter (CPC: Model 3771; TSI; d_{50} = 10 nm), a scanning mobility particle sizer (SMPS: Model 3080; TSI) consisting of a differential mobility analyser (long DMA: Model 3081; TSI) and a CPC (Model 3022A; TSI; d_{50} = 7 nm), an engine exhaust particle sizer (EEPS; TSI), and two sets of cascade impactor samplers (Nano MOUDI II: Model 125B; MSP Corp., Shoreview, MN, USA). The UCPC and CPC used for the field measurements are the same as those used for airborne measurements in our previous studies (Takegawa and Sakurai, 2011; Takegawa et al., 2014; Takegawa et al., 2017; Takegawa et al., in press). Number concentrations of aerosol particles with diameters larger than 2.5 nm or 10 nm, as measured by the UCPC or CPC, are referred to as $N_{2.5}$ or N_{10}, respectively. Details of the performance of the UCPC and CPC will be described later. The other instruments included a carbon dioxide (CO_2) monitor (Model 840; LI-COR Bioscience, Lincoln, NE, USA), a nitrogen oxides (NO_x) monitor, meteorological sensors, and a video camera for monitoring aircraft passages. We used data from the UCPC, CPC, SMPS, EEPS, and CO_2 monitor recorded from February 15 through February 22, 2018, for the present analysis. Although NO_x data are useful for characterizing aircraft emissions,

https://doi.org/10.5194/acp-2020-395
Preprint. Discussion started: 13 May 2020


Atmospheric Chemistry and Physics Discussions

we did not use those data because the response time was not sufficient to capture rapid changes in concentration in aircraft plumes.

Fig. 2 illustrates a schematic diagram of the sampling setup for the UCPC, CPC, SMPS, and CO_2. Ambient air was drawn into the container through a stainless-steel tube (ID: 10 mm; length: ~3 m) and was split into a bypass flow connecting to a piston pump and sample flows for aerosol and CO_2 measurements. The total flow rate through the main tube (the sum of the bypass and sample flows) was ~20 L min^{-1}. The aerosol sample flow was diluted by a factor of ~5 by using particle-free air (~2 L min^{-1}) to extend the concentration range measured by the UCPC and CPC, which would otherwise have been limited by particle-coincidence effects. The diluted sample flow was then passed through an evaporation tube (stainless-steel tube; ID: 7.5 mm; length: ~300 mm) for heated sampling or through a bypass tube for unheated (room temperature) sampling. A thermocouple sensor was attached on the upstream part of the evaporation tube for the temperature control. The three-way valve was switched between unheated and heated modes every 8 h. We set the heater temperature to 250°C during February 7–9, 150°C during February 11–13 and 22–23, and 350°C during February 15–21. We used data obtained during unheated and 350°C-heated modes for the present analysis. The characterization of the 150 and 250°C heated modes is now ongoing and will be presented elsewhere. A copper tube (ID: 7.5 mm; length: ~600 mm) between the evaporation tube and the valve was used to cool the heated sample air. The sampling method for 350°C-heated N_{10} approximately corresponds to the standard procedure for measuring non-volatile particles described in SAE-ARP6320 (SAE, 2018), although we did not use a thermal denuder or a catalytic stripper so as to reduce diffusion loss of particles. The estimation of potential artifacts is described in the next section. The tube downstream of the three-way valve was split into individual sample flows for the UCPC (~1.4 L min^{-1}), CPC (~1 L min^{-1}), and SMPS (~0.3 L min^{-1}). The SMPS was disconnected from the dilution and heater section after February 18, and the flow rate settings were changed accordingly. Note that the flow rates that were critical for calculating the dilution factor were calibrated by using the standard flowmeter at the National Institute of Advanced Industrial Science and Technology (AIST). The dilution factor was estimated to be ~3.8 before February 18 and ~6.1 after that date. Furthermore, the residence time in the heated section was ~0.19 s before February 18 and ~0.21 s after that. These values are slightly shorter than the requirement for the residence time (>0.25 s) described in SAE-ARP6320 (SAE, 2018). After the SMPS had been disconnected, the CPC 3022 was connected directly to the main sampling tube upstream of the dilution/heater section. This permitted overall validation of the dilution method, because the maximum concentration range of the CPC 3022 was extended to 10^7 cm^{-3} by photometric detection. Although we used the dilution method to reduce the effects of particle coincidence, we frequently observed high number concentrations of particles (>10^5 cm^{-3}) downstream of the dilution section. The effects of particle coincidence were corrected by using the methods described by our previous studies (Takegawa and Sakurai, 2011; Takegawa et al., 2017). The correction factors were as high as ~40% at nominal (uncorrected) particle number concentrations of ~5×10^5 cm^{-3} and ~1.2×10^5 cm^{-3} for the UCPC and CPC, respectively. The uncertainty in the corrections would become larger at even higher concentrations.

As mentioned earlier, measurements of particles below ~20 nm by mobility size spectrometers might include large uncertainties (Wiedensohler et al., 2012). The major sources of uncertainties in the SMPS measurements originate from the

https://doi.org/10.5194/acp-2020-395
Preprint. Discussion started: 13 May 2020


Atmospheric Chemistry and Physics Discussions

corrections for charging efficiency and Brownian diffusion, the latter generally being more significant for nanoparticles. The Aerosol Instrument Manager (AIM) software provides correction tools for these factors. We have found that the number size distributions at diameters below 20 nm show non-negligible differences for different versions of the software. We used the AIM version 9.0 for the present analysis, with the diffusion loss correction turned on.

The EEPS was operated independently with the UCPC/CPC/SMPS inlet system and it measured unheated particle number size distributions during the entire period. Although the particle diameter range detectable by the EEPS extended from ~6 to 500 nm, our laboratory experiments have shown that the EEPS may significantly underestimate particle number concentrations below ~10 nm. Reduced detection efficiencies of sub-10 nm particles can also be inferred from EEPS data obtained by other investigators (Moore et al., 2017a). The evaluation of the EEPS is now ongoing and will be presented elsewhere. In this study we used EEPS data for particle diameters larger than 10 nm.

The CO_2 instrument was calibrated by using two CO_2 standards (397.2 and 1032 ppmv) twice a day during the measurement period. The injection of the CO_2 standards was performed automatically by using solenoid valves. We found that the sensitivity of the instrument was generally stable during the measurement period.

The $N_{2.5}$, N_{10}, EEPS, and CO_2 data were obtained every 1 s, and the SMPS data were obtained every 5 min (scanning time: 3 min). When we observed spiked increases in particle number concentrations and CO_2 in aircraft plumes, the timing of the detection of concentration peaks did not exactly match among the individual instruments. Because this was likely caused by differences in the response time of the instruments and delay time in the sampling tubes, the data was shifted accordingly (<~10s).

2.2 Potential artifacts

Potential artifacts due to nucleation and growth of vaporized compounds after the evaporation tube are evaluated. Predicting the nucleation rates requires an estimate of the supersaturation of nucleating compounds, which is highly uncertain. Here we evaluate the growth rate of nucleated clusters under a given condition. The upper limit of this effect can be estimated by assuming that the number concentration of the vaporized compounds remains constant after a certain period of time (~1 s) and that all of the compounds are condensed onto nucleated clusters (e.g., sulphuric acid). In real situations, only a small fraction of the vaporized compounds might act as condensational growth of particles because of possible increases in their saturation vapour pressures by thermal decompositions and their deposition onto the inner surface of the sampling tube.

Let us assume a condensable material (number concentration of molecules: c; molecular weight: MW) in the gas-phase vaporized from particles. The original mass concentration in the particle phase before heating, m, is expressed as follows:

$$m = \frac{MW}{N_A} c \qquad (1)$$

https://doi.org/10.5194/acp-2020-395
Preprint. Discussion started: 13 May 2020


Atmospheric Chemistry and Physics Discussions

where N_A is the Avogadro number. Assuming a kinetic regime, the growth of nucleated particles is governed by the following expression (Seinfeld and Pandis, 2006):

$$\frac{\pi}{2}\rho D_p^2 \frac{dD_p}{dt} = \frac{MW}{N_A}\frac{\pi}{4} D_p^2 \bar{v}\alpha(c - c_{eq}) \qquad (2)$$

where ρ is the particle density, D_p is the diameter of nucleated particles, $\bar{v}$ is the mean thermal velocity of condensable gas molecules, α is the accommodation coefficient, and c_{eq} is the equilibrium number concentration. Assuming $\alpha = 1$ and $c_{eq} = 0$ (maximum molecular flux), we obtain this expression:

$$\frac{dD_p}{dt} = \frac{\bar{v}}{2\rho} m \qquad (3)$$

If we consider sulfuric acid as a condensable material, dD_p/dt (m s^{-1}) can be approximated as $0.1m$ at 350°C (the maximum gas temperature), where m is expressed in units of kg m^{-3}. The residence time for particle growth after the evaporation tube is estimated to be <1 s. The residence time of 1 s and the dilution factor of 5 lead to an estimate that the maximum particle growth is 1 nm at an ambient mass concentration of 50 μg m^{-3}. The minimum particle diameter at which the detection efficiency becomes zero are ~2 and ~7 nm for the UCPC and CPC, respectively (Takegawa and Sakurai, 2011; Takegawa et al., 2017). If we assume an initial cluster size of 1 nm, the effects of the artifacts on $N_{2.5}$ would be significant in aircraft exhaust plumes with relatively high concentrations (>~50 μg m^{-3}), and those on N_{10} (and SMPS) would be significant at very high concentrations (>~300 μg m^{-3}). This estimate does not change significantly if we assume high-molecular-weight organic compounds from jet-engine lubrication oil (slower thermal velocities and smaller particle densities compared with sulfuric acid).

2.3 Laboratory experiments

The accuracy of the measurements of particle number concentrations was the key issue in this study and this was evaluated in the laboratory at AIST before and after the field measurements. We mainly used the data obtained after the field measurements because they were more comprehensive than those obtained before the measurements. The test items included the size-resolved detection efficiencies of the UCPC and CPC, the penetration efficiency of non-volatile particles through the dilution/heater section, and the removal efficiency of volatile compounds through the evaporation tube.

An electrospray aerosol generator (EAG: Model 3480; TSI), a combustion aerosol standard (CAST; Matter Engineering, AG, Wohlen, Switzerland) with a tube furnace for thermal treatment at 350°C, and a custom-made tube furnace for supply of condensable vapours were used to generate polydisperse aerosol particles for the calibrations. We used sucrose particles supplied from the EAG for the detection efficiency experiment, non-volatile propane soot particles supplied from the CAST

https://doi.org/10.5194/acp-2020-395
Preprint. Discussion started: 13 May 2020


Atmospheric Chemistry and Physics Discussions

for the penetration efficiency experiment, and tetracontane ($C_{40}H_{82}$) particles supplied from the tube furnace particle generator for the removal efficiency experiment.

The experimental apparatus for measuring size-resolved detection efficiencies of the UCPC and CPC was similar to those used in our previous studies (Takegawa and Sakurai, 2011; Takegawa et al., 2017), except that the sampling lines were somewhat longer. The lengths of the sampling lines were limited by the instrument layout in the observation rack. Fig. 3 shows the experimental apparatus for testing the penetration and removal efficiencies. We set particle diameters at 15, 30, 50, and 100 nm for testing the penetration efficiency and at 15 and 30 nm for testing the removal efficiencies, in accord with the SAE-ARP6320 protocol. We used an aerosol electrometer (AE: Model 3068B; TSI) and a reference CPC (ref CPC: Model 3775; TSI) as reference instruments. These were calibrated with the standard AE maintained by AIST for particle number concentrations at ambient pressure in the size range 10–300 nm.

We also tested the removal efficiency of $C_{40}H_{82}$ particles for diameters of 30 and 50 nm in the laboratory at Tokyo Metropolitan University using a similar experimental setup as shown in Fig. 3. We used another CPC (Model 3772; TSI), which is essentially the same as a CPC Model 3771, for the detection of residual particles after the evaporation tube. An additional pump was used to maintain a flow rate of ~2.7 L min^{-1} through the evaporation tube.

3 Results

3.1 Laboratory experiments

Fig. 4a shows size-resolved detection efficiencies of the UCPC and CPC measured at AIST. The detection efficiencies for the UCPC and CPC were empirically estimated by using our previous calibration results for the CPC (Takegawa and Sakurai, 2011), the manufacturer's specification for the UCPC (Takegawa et al., 2017), and penetration efficiencies in the instrument (for the UCPC) and sampling lines. The penetration efficiencies were calculated by using the theoretical formulae proposed by Gormley and Kennedy (1949). We found a good agreement between the experimental data and the estimated detection efficiencies.

Fig. 4b shows the penetration and detection efficiency of non-volatile soot particles through the 350°C-heated-mode sampling tubes as measured by the UCPC. The temperature was set at room temperature and to 350°C for comparison. The penetration and detection efficiency includes the penetration efficiency through the dilution/heater section and the detection efficiency of the UCPC shown in Fig. 4a. Based on the specification required by the SAE-ARP6320 protocol, the penetration efficiency should be higher than or equal to 30, 55, 65, or 70% for particle diameters of 15, 30, 50, and 100 nm, respectively. Our data show that the penetration efficiency was well above the required specification for all diameters tested. Because a theoretical prediction of the penetration efficiency at 350°C is not straightforward, we scaled the penetration efficiency curve at room temperature to match the values observed at 350°C for larger diameters (30, 50, and 100 nm). For the removal efficiency test, we confirmed that the removal efficiencies of $C_{40}H_{82}$ particles for diameters of 15 and 30 nm were >99.9% (both by the UCPC and CPC) and that for 50 nm was >99% (by the CPC 3772). Although there are uncertainties in the

https://doi.org/10.5194/acp-2020-395
Preprint. Discussion started: 13 May 2020


Atmospheric Chemistry and Physics Discussions

actual gas temperature inside the evaporation tube, the removal efficiencies of $C_{40}H_{82}$ particles in our system are found to be comparable to those required by the SAE-ARP 6320 protocol.

3.2 Field observations

3.2.1 Particle number concentrations

Fig. 5 shows time series of $N_{2.5}$ and CO_2 obtained on February 15, 2018. The inlet valve was switched from the unheated to the 350°C-heated mode at 16:00 local time (LT). The wind directions were east or east-southeast for Fig. 5a and east or east-northeast for Fig. 5b (i.e., the winds were from the direction of the runway). The ambient temperature was ~10°C for Fig. 5a and ~8°C for Fig. 5b. We did not observe significant enhancement of aerosols or CO_2 when air parcels originated from the opposite direction from the runway during aircraft operating times (06:00-23:00 LT). The spikes in the concentrations of aerosol particles and in CO_2 shown in Fig. 5 can be interpreted as resulting from diluted exhaust plumes from individual aircraft. The observed values of $N_{2.5}$ (and N_{10}) for the 350°C-heated mode (Fig. 5b) were significantly lower than those for the unheated mode (Fig. 5a) when we compare plumes with similar enhancement levels of CO_2. The depletions of $N_{2.5}$ (and N_{10}) for the 350°C-heated mode were much larger than those expected from the difference in the penetration efficiency of aerosol particles between the unheated and the 350°C-heated modes (see Fig. 4), suggesting that most of the aerosol particles were volatile. We have previously shown that jet-engine lubrication oil was the major source of aerosol particles with diameters ranging from ~10 to 30 nm in air parcels observed during the measurement period (Fushimi et al., 2019). A key point in Fig. 5 is that the number fraction of particles with diameters ranging from 2.5 to 10 nm (red area) was generally larger than that of particles with sizes above 10 nm (grey area), for both the unheated and 350°C-heated modes. The significance of sub-10 nm size ranges for total particles in diluted plumes is qualitatively consistent with the findings from previous studies conducted on the ground (e.g., Petzold et al., 2005; Lobo et al., 2015b) or in-flight at cruise altitudes (Petzold et al., 1999; Kärcher et al., 2000; Brock et al., 2000), but that for non-volatile particles found in this study is unexpected.

Fig. 6 is a scatterplot of 1 s averaged values of N_{10} versus those of $N_{2.5}$ for the 350°C-heated mode for time period 17:00 to 23:00 on February 15, 2018, the same data as used in Fig. 5b. Data obtained on February 21, 2018 at slightly different flow rate settings (see section 2.1) are also plotted to show the reproducibility of the results. The 1:1 correspondence line ($N_{10} = N_{2.5}$) represents the state in which all particles are included in the size range larger than 10 nm, and deviations below the 1:1 line indicate that the fractions of sub-10 nm particles increase. These results show that many data points lie below the 1:2 line (sub-10 nm fraction of >50%) when $N_{2.5}$ exceeds ~10^5 cm^{-3}. Specifically, some data points were found on the 1:10 correspondence line (sub-10 nm fraction of ~90%). The deviations from the 1:1 line would have been even larger had we considered the size-dependent loss of particles in the sampling line shown in Fig. 4.

https://doi.org/10.5194/acp-2020-395
Preprint. Discussion started: 13 May 2020


Atmospheric Chemistry and Physics Discussions

3.2.2 Size distributions of total particles

Fig. 7 shows time series of total particle number concentrations measured by the CPC and EEPS and particle number and volume size distributions ($dN/d\log D$ and $dV/d\log D$) as measured simultaneously by the EEPS and unheated SMPS for selected time periods on February 15, 2018. The total particle number concentrations measured by the CPC and EEPS showed reasonable agreement, which confirms the overall consistency between these two independent measurements. The time periods were selected carefully to investigate the effects of rapid changes in the particle number concentration during each SMPS scan on the derived particle size distribution. The SMPS needed ~30 s to scan the major population of particle number concentrations in aircraft plumes (<30 nm). Considering possible delays in the detection timing due to the residence time in the SMPS sampling tubes (<5 s), the EEPS data were averaged over 40 s around the timing of the SMPS scan corresponding to the diameter range of 15–30 nm (i.e., averaged from 10 s before to 30 s after the onset of each SMPS scan). For the SMPS scan at 14:10 LT, the particle number concentration varied by a factor of ~2 during the first 30-s scan time, but there was no systematic increase or decrease in the particle number concentration. We have found a reasonable agreement between the EEPS and SMPS (within a factor of ~2). For the SMPS scan at 14:20 LT, the particle number concentration decreased significantly during the 30-s scan time, and then started to increase rapidly afterwards. The resultant number size distribution was likely affected by these concentration changes. These results demonstrate that the SMPS data can be used to investigate the characteristics of particle size distributions within specific size ranges by selecting appropriate time windows.

In the enhancement events at 14:10 and 14:20 LT in Fig. 7, the EEPS data indicate that the particle number size distribution functions below ~50 nm showed significant increases compared with that in the non-enhancement event (14:00 LT). The particle volume size distribution function below ~50 nm exhibited moderate increases in the enhancement events, but the total integrated particle volume concentrations were largely affected by accumulation-mode particles (>50 nm) in background air. A similar feature was also found for other time periods (Fushimi et al., 2019; Misawa et al., manuscript in preparation).

3.2.3 Size distributions of non-volatile particles

Fig. 8 shows particle number and volume size distributions as measured simultaneously by the EEPS and 350°C-heated SMPS for selected time periods with and without enhancements of aerosol particle number concentrations on February 15, 2018. The time periods were selected so that there was no systematic increase or decrease in the particle number concentrations during the first 30-s scan time of the SMPS. Similarly to Fig. 7, the particle number size distribution functions below ~50 nm in the enhancement events showed significant increases compared with that in the non-enhancement event for both the EEPS and 350°C-heated SMPS. The particle number size distribution functions below ~50 nm measured by the 350°C-heated SMPS were smaller by more than an order of magnitude than those by the EEPS, indicating that aircraft exhaust particles were mostly volatile below ~50 nm. Although we did not test the removal efficiency of particles with

https://doi.org/10.5194/acp-2020-395
Preprint. Discussion started: 13 May 2020


Atmospheric Chemistry and Physics Discussions

diameters larger than 50 nm, "residues" of larger particles (>50 nm) after the evaporation tube were likely negligible because the particle number concentrations for a diameter range of >50 nm measured by the EEPS were far below the observed values of 350°C-heated N_{10} (Fig. 8a).

Effects of nucleation artifacts (section 2.2) might be a major concern but were likely small under the observation conditions because the mass concentrations of aerosol particles in aircraft plumes inferred from Fig. 8 were much lower than the threshold concentration (~50 μg m^{-3}) described in section 2.2. In fact, we did not find any systematic increases in $N_{2.5}/N_{10}$ ratios for the 350°C-heated mode with increasing total particle volume concentrations derived from the EEPS (not shown). Furthermore, the particle number and volume size distributions derived from the 350°C-heated SMPS (Figs. 8b-c) exhibited no indication of the presence of artificial nucleation mode. The $dN/d\log D$ functions in Fig. 8b exhibited gradual increasing trends with decreasing particle diameters from ~100 to ~15 nm, which is unlikely explained by nucleation artifacts.

3.2.4 Particle emission indices for take-off plumes

The temporal variations and number size distributions of aerosol particles clearly indicate that the observed air parcels were significantly affected by aircraft emissions under appropriate wind conditions. However, aircraft emissions from various cycles of take-off, landing, and idling may have been mixed in the atmosphere. We calculated enhancements of $N_{2.5}$, N_{10}, and CO_2 above the background levels (referred to as $\Delta N_{2.5}$, ΔN_{10}, and ΔCO_2, respectively), and extracted discrete plumes during take-off phases by setting some criteria for these parameters (see section S1 and Figs. S1–S3 in the Supplement for details). By using the data obtained on February 15, 16, 20, 21, and 22, we identified 132 discrete plumes for the unheated mode and 63 for the 350°C-heated mode. Particle number and volume size distributions ($dN/d\log D$ and $dV/d\log D$) for the take-off plumes were derived from the EEPS data (unheated conditions), and the enhancements of $dN/d\log D$ and $dV/d\log D$ above background levels were calculated using the same method as $\Delta N_{2.5}$.

The $\Delta N_{2.5}/\Delta CO_2$ and $\Delta N_{10}/\Delta CO_2$ ratios were converted into particle number EIs by assuming a CO_2 EI value of 3160 g of CO_2 per kilogram of fuel (Moore et al., 2007a; see Table 1). Corrections for the penetration and detection efficiencies of the UCPC and CPC were not incorporated into the above estimates because the actual size distributions were uncertain; these values should therefore be regarded as lower limits. We did not find systematic dependence of the $\Delta N_{10}/\Delta CO_2$ and $\Delta N_{2.5}/\Delta CO_2$ ratios on the estimated arrival time of plumes (see Fig. S3 in the Supplement), suggesting that variation of plume ages did not yield significant biases in our results. We did not perform detailed classification of the plumes by jet engine types because information on the engines of the aircraft observed at NRT was not available. We performed simple classification of the plumes by aircraft models (see Table S1 in the Supplement), but did not find significant differences among different types of aircraft.

The median total EI($N_{2.5}$) was ~60 times larger than the median non-volatile EI(N_{10}). This value can be interpreted as the difference between total particle number emissions under real-world conditions and non-volatile particle number emissions regulated by standard engine tests (SAE, 2018). Although the fact that particle emissions under real-world

https://doi.org/10.5194/acp-2020-395
Preprint. Discussion started: 13 May 2020


Atmospheric Chemistry and Physics Discussions

conditions are larger than those measured during standard engine tests is well-known, few studies have reported quantitative estimates of the difference.

We defined sub-10 nm fraction as $1–\Delta N_{10}/\Delta N_{2.5}$ for the identified discrete plumes. The median and central 50 percentile range of the sub-10 nm fraction for the unheated mode were found to be 0.63 and 0.53–0.70, respectively, and those for the 350°C-heated mode were 0.54 and 0.44–0.72, respectively (Table 1). The significance of sub-10 nm particles for total and non-volatile particles, which was shown in section 3.2.1–3.2.3 (Figs. 5–8) as a case study, was also found in the statistical analysis of the take-off plumes.

Lobo et al. (2015b) reported particle number and mass EIs measured near jet engine exits and 100–350 m downwind of runways at Hartsfield-Jackson Atlanta International Airport. The former corresponds to non-volatile particle EIs and the latter corresponds to total particle EIs. They used a fast particulate spectrometer (DMS500, Cambustion) to measure particle number size distributions with diameters ranging from 5 to 1000 nm. The non-volatile particle number EIs for a JT8D-219 engine were ~1×10^{16} kg-fuel^{-1} under 85 and 100% thrust conditions, which were close to the 75 percentile value of non-volatile EI($N_{2.5}$) from our measurements. Based on Fig. 7 of Lobo et al. (2015b), the medians of total particle number EIs for various types of engines under take-off conditions ranged from ~5×10^{16} to ~3×10^{17} kg-fuel^{-1}, which inclusively covered the 25-75 percentile range of total EI($N_{2.5}$) from our measurements.

Moore et al. (2017a) reported particle number and volume EIs for take-off plumes based on field observations at Los Angeles International Airport (LAX), and provided useful dataset that can be directly compared with our results. They used a CPC 3775 (d_{50} = 4 nm) for the measurements of total particles, a CPC 3022A (d_{50} = 7 nm) for non-volatile particles, and an EEPS for the measurements of size distributions. The median values of the total and non-volatile particle number EIs listed in Table 4 of Moore et al. (2017a) were calculated to be 3.4×10^{16} and 1.9×10^{15} kg-fuel^{-1}, which were comparable to the median values of the total and non-volatile EI(N_{10}) from our measurements. Zhang et al. (2019) reported an average non-volatile particle number EI (diameter >10 nm) of 6.06×10^{14} kg-fuel^{-1} for various conditions of engine thrust. The average value from Zhang et al. (2019) is significantly smaller than the median non-volatile particle number EIs from Moore et al. (2017a) and from our measurements. The median non-volatile EI($N_{2.5}$) from our measurements, which may inclusively cover the size range relevant to aircraft emissions, is larger by nearly an order of magnitude than the non-volatile particle number EIs reported by Zhang et al. (2019).

3.2.5 Size distributions of total particles for take-off plumes

The enhancements $dN/d\log D$ and $dV/d\log D$ above background levels derived from the EEPS data were converted to the corresponding EI values ($d\mathrm{EI}(N)/d\log D$ and $d\mathrm{EI}(V)/d\log D$). Fig. 9 shows the size distributions of total particle number and volume EIs for the take-off plumes. It should be noted that the quality of data at larger particle diameters (>~100 nm) was not sufficient because they were significantly affected by accumulation-mode particles in background air. The size distributions of particle number and volume EIs for take-off plumes observed at LAX (Moore et al., 2017a), which are characterized by bimodal log-normal distributions (nucleation and soot modes), are shown for comparison. The mode

https://doi.org/10.5194/acp-2020-395
Preprint. Discussion started: 13 May 2020


Atmospheric Chemistry and Physics Discussions

diameters of $d\mathrm{EI}(N)/d\log D$ for nucleation mode reported by Moore et al. (2017a) ranged from ~10 to 20 nm. Fig. 9 suggests that the mode diameters of $d\mathrm{EI}(N)/d\log D$ for nucleation-mode particles obtained in this study were smaller than ~10 nm, and that the peak values of $d\mathrm{EI}(N)/d\log D$ were larger than those reported by Moore et al. (2017a).

Other previous studies also reported that the mode diameters of particle number EIs generally ranged from ~10 to 20 nm under high engine thrust conditions (e.g., Kinsey, 2009; Yu et al., 2017, 2019). An exception is Kinsey et al. (2019), who investigated the emission characteristics of a commercial gas turbine engine (CFM56-2C1) onboard a DC-8 with blending two types of fuels (military JP-8 and Fischer-Tropsch: FT) under various thrust conditions and ambient temperatures. The sulphur content of fuels for the FT-fuels were much lower than that for the JP-8 fuels. They found that the mode diameters of $d\mathrm{EI}(N)/d\log D$ under high engine thrust exhibited strong dependence on the fuel composition and weak dependence on ambient temperatures. They observed mode diameters of <10 nm under high thrust conditions with the use of FT fuels, although the peak values of $d\mathrm{EI}(N)/d\log D$ (~10^{16} $\mathrm{cm^{-3}}$ $\mathrm{kg\text{-}fuel^{-1}}$) were far lower than those found in this study.

4 Discussion

We estimate possible particle number size distributions for total and non-volatile particles constrained by the UCPC and CPC observations. We assumed log-normal number size distributions with various geometric mean diameters (GMDs) and geometric standard deviations (GSDs). We calculated the number fraction of sub-10 nm particles ($1 - \Delta N_{10}/\Delta N_{2.5}$) by integrating the number size distributions weighted by the penetration and detection efficiency curves:

$$\text{Calculated sub-10 nm fraction} = 1 - \left(\int \eta_{10}(\log D_p)\, n(\log D_p)\, d\log D_p\right) \Big/ \left(\int \eta_{2.5}(\log D_p)\, n(\log D_p)\, d\log D_p\right) \quad (4)$$

where η_{10} and $\eta_{2.5}$ are the overall penetration and detection efficiencies for N_{10} and $N_{2.5}$, respectively, and n is the assumed number size distribution function. The overall penetration efficiency, which included the sampling tubes from the rooftop and dilution/heater sections (see Fig. 2 and Fig. 4b), was calculated based on the theoretical formulae by Gormley and Kennedy (1949). Fig. 10 shows the calculation results. For total particles, GMD values of <~10 nm are needed to explain the median sub-10 nm fraction derived from the plume analysis (0.63) with a realistic range of GSDs (1.2–1.6). These results are consistent with the measurements by the EEPS (Fig. 9), which supports the validity of our estimate. Fushimi et al. (2019) found the importance of jet engine lubrication oil as a source of aircraft exhaust particles with diameters ranging from ~10 to 30 nm. An important question arises from how lubrication oil contributes to the formation and growth of sub-10 nm particles. Future researches addressing this issue would be useful for developing a method for reducing particle emissions from aircraft.

For non-volatile particles, GMD values of <~10 nm would also be needed to explain the median sub-10 nm fraction derived from the plume analysis (0.54), although the size distribution data to support the validity of this estimate are limited. This feature is significantly different from the soot mode size distributions reported by previous studies (Petzold et al., 1999,

https://doi.org/10.5194/acp-2020-395
Preprint. Discussion started: 13 May 2020


Atmospheric Chemistry and Physics Discussions

Lobo et al., 2015a, Zhang et al., 2019). Our estimate implies the presence of very small soot particles with diameters down to a few nm. This is not consistent with the size of primary soot particles from jet engines estimated by using transmission electron microscope (TEM) or laser-induced incandescence (LII) methods (e.g., Liati et al., 2014; Boies et al., 2015; Saffaripour et al., 2017, 2020), although there still remain substantial uncertainties in estimating the size of primary particles by those methods, as pointed out by Boies et al. (2015).

Currently we do not have direct evidences that the observed sub-10 nm non-volatile particles are composed mainly of soot. Nevertheless, it is worthwhile considering potential formation mechanisms of sub-10 nm soot particles. In general, the formation processes of soot particles from combustion sources are complicated and not fully understood (Johansson et al., 2018; Commodo et al., 2019). The whole mechanism, including inception and growth, takes place at high temperatures and on timescales of the order of a few milliseconds; moreover, sub-10 nm soot particles can be generated during the early stages of formation processes (Commodo et al., 2019). If combustion gases from jet engines immediately expand and are diluted on a timescale comparable to that for the formation of soot, significant numbers of sub-10 nm soot particles might be emitted to the atmosphere without the formation of larger agglomerates.

An alternative possibility for the significance of sub-10 nm non-volatile particles includes potential contributions of less volatile organic matters (as compared with $C_{40}H_{82}$) or metal compounds. Fushimi et al. (2019) showed that the mass contribution of the sum of trace elements (other than carbonaceous and sulphur compounds) was comparable to that of elemental carbon (soot) for UFP samples (~10-30 nm) collected at NRT. Saitoh et al. (2019) presented that metal elements including Ca, Fe, Si, Mg, K, Zn, Pb, and Ni were the major compositions of these trace elements. Further investigations are needed to quantify the contributions of metal compounds to particle number concentrations.

5 Conclusions and Implications

We conducted field measurements of aerosols at an observation point ~180 m from the centreline of a runway of Narita International Airport. We investigated the characteristics of particle emissions from in-use commercial aircraft under real-world operating conditions, with specific focuses on the contributions of sub-10 nm size ranges to total and non-volatile (350°C-heated) particles. The major conclusions are summarized below.

- The median total EI($N_{2.5}$) was ~60 times larger than the median non-volatile EI(N_{10}) for the take-off plumes. This value can be interpreted as the difference between total particle number emissions under real-world conditions and non-volatile particle number emissions regulated by standard engine tests.
- More than half of total and non-volatile particle number EIs in aircraft take-off plumes were found in the size range smaller than ~10 nm on average. The median sub-10 nm fraction in the plumes was calculated to be 0.63 and 0.54 for total and non-volatile particles, respectively.

https://doi.org/10.5194/acp-2020-395
Preprint. Discussion started: 13 May 2020


Atmospheric Chemistry and Physics Discussions

- The UCPC, CPC, and EEPS data consistently suggest that the mode diameters of $d\mathrm{EI}(N)/d\log D$ for nucleation-mode particles obtained in this study were smaller than ~10 nm, and that the peak values of $d\mathrm{EI}(N)/d\log D$ were larger than those previously reported under real-world operating conditions.
- The 350°C-heated UCPC, CPC, and SMPS data suggest that the contributions of sub-10 nm size ranges to non-volatile particle number EIs might be much higher than previously considered. Direct measurements of chemical compositions of sub-10 nm particles are needed to investigate the mechanisms.

It should be noted that the characteristics of particle emissions may significantly depend on the type of jet engines, their maintenance conditions, and sulphur content of fuels, which are not available in this study. Particle emissions may also depend on other factors including ambient pressure and temperature. These factors should be carefully considered for more systematic comparison among different studies.

Although the potential contributions of sub-10 nm particles inferred from our results likely have small impacts on the mass concentrations of ambient aerosol particles, they may have non-negligible impacts on the number concentrations in and around airports and also at aircraft cruising altitudes. The lifetime of sub-10 nm particles would be short near the ground level due to evaporative loss (e.g., Fushimi et al., 2008) and/or coagulation scavenging onto pre-existing larger particles, but it could be much longer under conditions of low temperatures and reduced concentrations of pre-existing aerosol particles. We propose that emissions of sub-10 nm particles from aircraft under real-world conditions should be properly considered for understanding aviation impacts on human health and also for developing aviation emission inventories for regional and global models.

Data availability

The field measurement data used in this study are provided as a supplementary material and will be available at a data repository.

Author contributions

NT, AF, and HS designed research; NT, AF, KM, YF, and KS performed field observations and collected data; NT, YM, HS performed laboratory experiments; NT and YM performed data analysis; NT, AF, YF, and HS wrote the paper.

Competing interests

The authors declare no conflict of interest.

https://doi.org/10.5194/acp-2020-395
Preprint. Discussion started: 13 May 2020

Atmospheric Chemistry and Physics Discussions

Acknowledgments

We thank Narita International Airport Corporation and Narita International Airport Promotion Foundation for their help during the field observations at Narita International Airport. We also thank Takumi Saotome at Research Institute for Environmental Strategies, Inc., Makiko Mine and Anna Nagasaki at Tokyo Metropolitan University for their help in the observations and data analysis, and Kenjiro Iida at AIST for useful advices on the evaluation of the UCPC and CPC. This study was funded by the Environment Research and Technology Development Fund (5-1709) of the Ministry of the Environment, Japan.

References

Boies, A. M., Stettler, M. E. J., Swanson, J. J., Johnson, T. J., Olfert, J. S., Johnson, M., Eggersdorfer, M. L., Rindlisbacher, T., Wang, J., Thomson, K., Smallwood, G., Sevcenco, Y., Walters, D., Williams, P. I., Corbin, J., Mensah, A. A., Symonds, J., Dastanpour, R., and Rogak, S. N., Particle emission characteristics of a gas turbine with a double annular combustor, Aerosol Sci. Technol., 49, 842-855, 2015.

Brock, C. A., Schröder, F., Kärcher, B., Petzold, A., Busen, R., and Fiebig, M.: Ultrafine particle size distributions measured in aircraft exhaust plumes, J. Geophys. Res., 105, 26555–26567, 2000.

Commodo, M., Kaiser, K., De Falco, G., Minutolo, P., Schulz, F., D'Anna, A., and Gross, L.: On the early stages of soot formation: Molecular structure elucidation by high-resolution atomic force microscopy, Combust. Flame, 205, 154–164, 2019.

Durdina, L., Brem, B. T., Schönenberger, D., Siegerist, F., Anet, J. G., and Rindlisbacher, T.: Nonvolatile particulate matter emissions of a business jet measured at ground level and estimated for cruising altitudes, Environ. Sci. Technol., 53, 12865–12872, 2019.

Fushimi, A., Hasegawa, S., Takahashi, K., Fujitani, Y., Tanabe, K., and Kobayashi, S.: Atmospheric fate of nuclei-mode particles estimated from the number concentrations and chemical composition of particles measured at roadside and background sites, Atmos. Environ., 42, 949–959, 2008.

Fushimi, A., Saitoh, K., Fujitani, Y., and Takegawa, N.: Identification of jet lubrication oil as a major component of aircraft exhaust nanoparticles, Atmos. Chem. Phys., 19, 6389–6399, 2019.

Gormley, P. G., and Kennedy, M.: Diffusion from a stream flowing through a cylindrical tube, Proc. Royal Irish Acad. Sect. A, 52, 163–169, 1949.

Hagen, D. E., Whitefield, P. D., Paladino, J. D., and Trueblood, M. B.: Particulate sizing and emission indices for a jet engine exhaust sampled at cruise, Geophys. Res. Lett., 25, 1681–1684, 1998.

Herndon, S. C., Jayne, J. T., Lobo, P., Onasch, T. B., Fleming, G., Hagen, D. E., Whitefield, P. D., and Miake-Lye, R. C.: Commercial aircraft engine emissions characterization of in-use aircraft at Hartsfield-Jackson Atlanta International Airport, Environ. Sci. Technol., 42, 1877–1883, 2008.

https://doi.org/10.5194/acp-2020-395
Preprint. Discussion started: 13 May 2020


Atmospheric Chemistry and Physics Discussions

International Civil Aviation Organization, "Doc 10075. Assembly Resolutions in Force (as of 6 October 2016)" (ICAO, 2017; https://www.icao.int/Meetings/a39/Documents/Resolutions/10075_en.pdf).

Johansson, K. O., Head-Gordon, M. P., Schrader, P. E., Wilson, K. R., and Michelsen, H. A.: Resonance-stabilized hydrocarbon-radical chain reactions may explain soot inception and growth, Science, 361, 997–1000, 2018.

Jonsdottir, H. R., Delaval, M., Leni, Z., Keller, A., Brem, B. T., Siegerist, F., Schönenberger, D., Durdina, L., Elser, M., Burtscher, H., Liati, A., and Geiser, M.: Non-volatile particle emissions from aircraft turbine engines at ground-idle induce oxidative stress in bronchial cells, Commun. Biol., 2, 90, 2019.

Kärcher, B., Turco, R. P., Yu, F., Danilin, M. Y., Weisenstein, D. K., Miake-Lye, R. C., Busen, R.: A unified model for ultrafine aircraft particle emissions, J. Geophys. Res., 105, 29379–29386, 2000.

Kärcher, B., and Voigt, C.: Susceptibility of contrail ice crystal numbers to aircraft soot particle emissions, Geophys. Res. Lett., 44, 8037–8046, 2017.

Kärcher, B.: Formation and radiative forcing of contrail cirrus, Nat. Commun., 9, 1824, 2018.

Kinsey, J. S.: "Characterization of emissions from commercial aircraft engines during the Aircraft Particle Emissions eXperiment (APEX) 1 to 3" (EPA-600, R-09,130, EPA, 2009; https://cfpub.epa.gov/si/).

Kinsey, J. S., Squier, W., Timko, M., Dong, Y., and Logan, R.: Characterization of the fine particle emissions from the use of two Fischer–Tropsch fuels in a CFM56-2C1 commercial aircraft engine, Energy Fuels, 33, 8821–8834, 2019.

Lee, D. S., Pitari, G., Grewe, V., Gierens, K., Penner, J. E., Petzold, A., Prather, M. J., Schumann, U., Bais, A., Berntsen, T., Iachetti, D., Lim, L.L., and Sausen, R.: Transport impacts on atmosphere and climate: Aviation, Atmos. Environ., 44, 4678-4734, doi:10.1016/j.atmosenv.2009.06.005, 2010.

Liati, A., Brem, B. T., Durdina, L., Vögtli, M., Dasilva, Y. A. R., Eggenschwiler, P. D., and Wang, J., Electron microscopic study of soot particulate matter emissions from aircraft turbine engines, Environ. Sci. Technol., 48, 10975-10983, 2014.

Lobo, P., Durdina, L., Smallwood, G. J., Rindlisbacher, T., Siegerist, F., Black, E. A., Yu, Z., Mensah, A. A., Hagen, D. E., Miake-Lye, R. C., Thomson, K. A., Brem, B. T., Corbin, J. C., Abegglen, M., Sierau, B., Whitefield, P. D., and Wang, J.: Measurement of aircraft engine non-volatile PM emissions: Results of the Aviation-Particle Regulatory Instrumentation Demonstration Experiment (A-PRIDE) 4 campaign, Aerosol Sci. Technol., 49, 472–484, 2015a.

Lobo, P., Hagen, D. E., Whitefield, P. D., and Raper, D.: PM emissions measurements of in-service commercial aircraft engines during the Delta-Atlanta Hartsfield Study, Atmos. Environ. 104, 237-245, doi: http://dx.doi.org/10.1016/j.atmosenv.2015.01.020, 2015b.

Masiol, M., and Harrison, R. M.: Aircraft engine exhaust emissions and other airport-related contributions to ambient air pollution: A review, Atmos. Environ., 95, 409–455, 2014.

Moore, R. H., Shook, M. A., Ziemba, L. D., DiGangi, J. P., Winstead, E. L., Rauch, B., Jurkat, T., Thornhill, K. L., Crosbie, E. C., Robinson, C., Shingler, T. J., and Anderson, B. E.: Take-off engine particle emission indices for in-service aircraft at Los Angeles International Airport, Sci. Data, 4, 170198, 2017a.

https://doi.org/10.5194/acp-2020-395
Preprint. Discussion started: 13 May 2020

Moore, R. H., Thornhill, K. L., Weinzierl, B., Sauer, D., D'Ascoli, E., Kim, J., Lichtenstern, M., Scheibe, M., Beaton, B., Beyersdorf, A. J., Barrick, J., Bulzan, D., Corr, C. A., Crosbie, E., Jurkat, T., Martin, R., Riddick, D., Shook, M., Slover, G., Voigt, C., White, R., Winstead, E., Yasky, R., Ziemba, L. D., Brown, A., Schlager, H., and Anderson, B. E.: Biofuel blending reduces particle emissions from aircraft engines at cruise conditions, Nature, 543,411–415, 2017b.

Oberdörster, G., Oberdörster, E., and Oberdörster, J.: Nanotoxicology: An emerging discipline evolving from studies of ultrafine particles, Environ. Health Perspect., 113, 823–839, 2005.

Onasch, T. B., Jayne, J. T., Herndon, S., Worsnop, D. R., Miake-Lye, R. C., Mortimer, I. P., and Anderson, B. E.: Chemical properties of aircraft engine particulate exhaust emissions, J. Propul. Power, 25, 1121–1137, 2009.

Petzold, A., Döpelheuer, A., Brock, C. A., and Schröder, F.: In situ observations and model calculations of black carbon emission by aircraft at cruise altitude,. J. Geophys. Res., 104, D18, 22171–22181, 1999.

Petzold, A., et al.: Particle emissions from aircraft engines - a survey of the European project PartEmis, Meteorologische Zeitschrift, 14, 465-476, 2005.

Righi, M., Hendricks, J., and Sausen, R.: The global impact of the transport sectors on atmospheric aerosol in 2030 - Part 2: Aviation, Atmos. Chem. Phys., 16, 4481–4495, 2016.

Saffaripour, M., Tay, L.-L., Thomson, K. A., Smallwood, G. J., Brem, B. T., Durdina L., and Johnson, M., Raman spectroscopy and TEM characterization of solid particulate matter emitted from soot generators and aircraft turbine engines, Aerosol Sci. Technol., 51, 518-531, 2017.

Saffaripour, M., Thomson, K. A., Smallwood, G. J., and Lobo, P., A review on the morphological properties of non-volatile particulate matter emissions from aircraft turbine engines, J. Aerosol Sci., 139, 105467, 2020.

Saitoh K., Fushimi A., Fujitani F., Morino Y., Saotome T., Takegawa N. and Sera K.: Elemental composition of jet lubricating oil and fuel, and particles (particle size 10 nm-10 μm) collected near the Narita International Airport runway, Nishina Memorial Cyclotron Center Annual Report, 24 (fiscal year 2017), 41-52, published in 2019 (in Japanese).

Seinfeld, J. H., and Pandis, S. N.: Atmospheric Chemistry and Physics: From Air Pollution to Climate Change (Wiley, Hoboken, NJ, 2nd ed., 2006).

Society of Automotive Engineers, "Procedure for the continuous sampling and measurement of non-volatile particulate matter emissions from aircraft turbine engines: - Aerospace recommended practice 6320" (SAE International, 2018; https://saemobilus.sae.org/content/ARP6320/#scope).

Stacey, B.: Measurement of ultrafine particles at airports: A review, Atmos. Environ., 198, 463–477, 2019.

Takegawa, N., and Sakurai, H.: Laboratory evaluation of a TSI condensation particle counter (Model 3771) under airborne measurement conditions, Aerosol Sci. Technol., 45, 272–283, 2011.

Takegawa, N., Moteki, N., Oshima, N., Koike, M., Kita, K., Shimizu, A., Sugimoto, N., and Kondo, Y.: Variability of aerosol particle number concentrations observed over the western Pacific in the spring of 2009, *J. Geophys. Res. Atmos.*, *119*, 13,474-13,488, doi:10.1002/2014JD022014, 2014.

https://doi.org/10.5194/acp-2020-395
Preprint. Discussion started: 13 May 2020

535 Takegawa, N., Iida, K., and Sakurai, H.: Modification and laboratory evaluation of a TSI ultrafine condensation particle counter (Model 3776) for airborne measurements, Aerosol Sci. Technol., 51, 235–245, 2017.

Takegawa, N., Seto, T., Moteki, N., Koike, M., Oshima, N., Adachi, K., Kita, K., Takami, A., and Kondo, Y.: Enhanced new particle formation above the marine boundary layer over the Yellow Sea: Potential impacts on cloud condensation nuclei, *J. Geophys. Res. Atmos.*, in press.

540 Timko, M. T., Onasch, T. B., Northway, M. J., Jayne, J. T., Canagaratna, M. R., Herndon, S. C., Wood, E. C., Miake-Lye, R. C., and Knighton, W. B.: Gas turbine engine emissions: Part II: Chemical properties of particulate matter, J. Eng. Gas Turbines Power, 132, 061505, 2010.

Westerdahl, D., Fruin, S. A., Fine, P. L., and Sioutas, C.: The Los Angeles International Airport as a source of ultrafine particles and other pollutants to nearby communities, Atmos. Environ., 42, 3143–3155, 2008.

545 Wiedensohler, A., Birmili, W., Nowak, A., Sonntag, A., Weinhold, K., Merkel, M., Wehner, B., Tuch, T., Pfeifer, S., Fiebig, M., Fjäraa, A. M., Asmi, E., Sellegri, K., Depuy, R., Venzac, H., Villani, P., Laj, P., Aalto, P., Ogren, J. A., Swietlicki, E., Williams, P., Roldin, P., Quincey, P., Hüglin, C., Fierz-Schmidhauser, R., Gysel, M., Weingartner, E., Riccobono, F., Santos, S., Grüning, C., Faloon, K., Beddows, D., Harrison, R., Monahan, C., Jennings, S. G., O'Dowd, C. D., Marinoni, A., Horn, H.-G., Keck, L., Jiang, J., Scheckman, J., McMurry, P. H., Deng, Z., Zhao, C. S., Moerman, M., Henzing, B.,
550 de Leeuw, G., Löschau, G., Bastian, S.: Mobility particle size spectrometers: Harmonization of technical standards and data structure to facilitate high quality long-term observations of atmospheric particle number size distributions, Atmos. Meas. Tech., 5, 657–685, 2012.

Yu, Z., Liscinsky, D. S., Fortner, E. C., Yacovitch, T. I., Croteau, P., Herndon, S. C., and Miake-Lye, R. C., Evaluation of PM emissions from two in-service gas turbine general aviation aircraft engines, Atmos. Environ., 160, 9-18, 2017.

555 Yu, Z., Timko, M. T., Herndon, S. C., Miake-Lye, R. C., Beyersdorf, A. J., Ziemba, L. D., Winstead, E. L., and Anderson, B. E., Mode-specific, semi-volatile chemical composition of particulate matter emissions from a commercial gas turbine aircraft engine, Atmos. Environ., 218, 116974, 2019.

Zhang, X., Chen, X., and Wang, J.: A number-based inventory of size-resolved black carbon particle emissions by global civil aviation, Nat. Commun., 10, 534, 2019.

https://doi.org/10.5194/acp-2020-395
Preprint. Discussion started: 13 May 2020

Atmospheric Chemistry and Physics Discussions

560

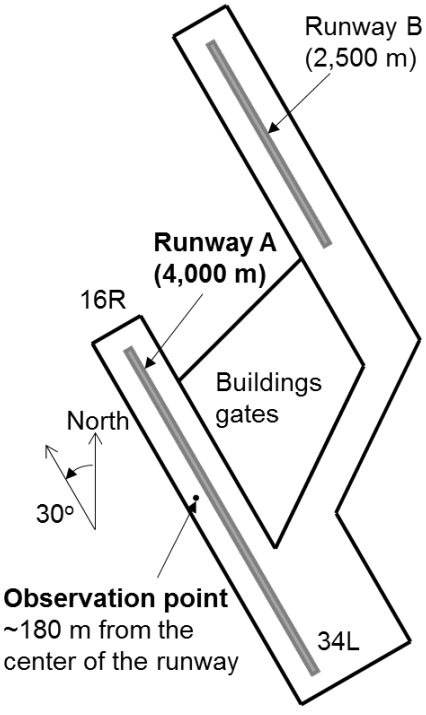

Figure 1: An approximate layout of Narita International Airport (NRT). The observation point was located ~180 m from the centerline of runway A (~140 m from the edge of the runway). The azimuth of runway A is 30° from north (23° from magnetic north). The photograph
565 shows the containers of instruments deployed at the observation point.

https://doi.org/10.5194/acp-2020-395
Preprint. Discussion started: 13 May 2020

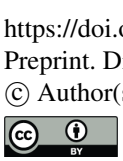

Atmospheric Chemistry and Physics Discussions

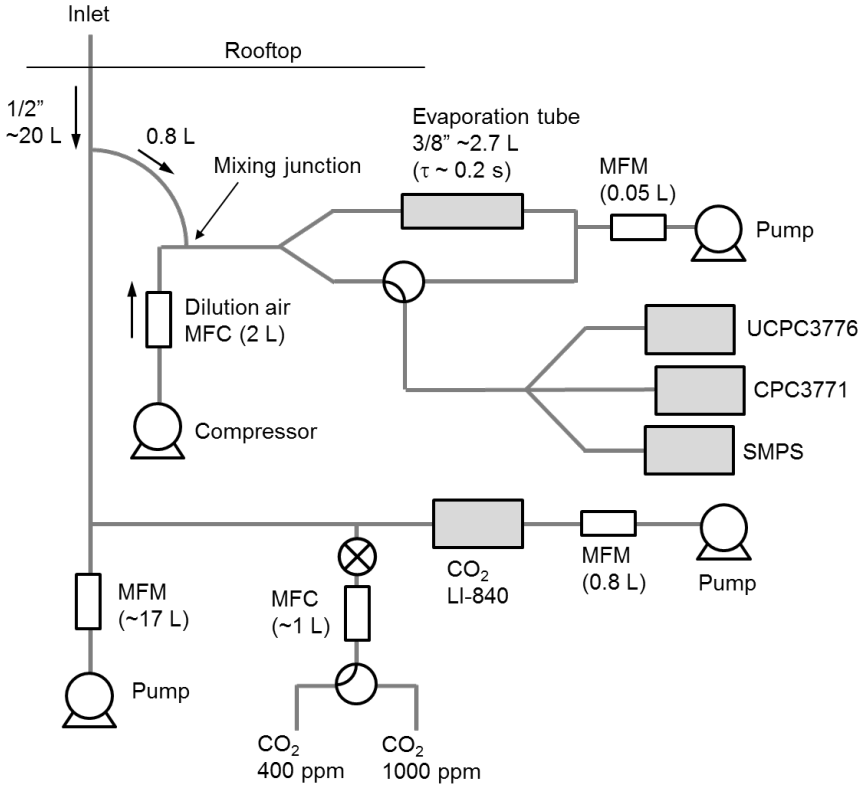

570 **Figure 2:** Schematic of the sampling setup. Ambient air was drawn into the container through a stainless steel tube and was split into a bypass flow connecting to a piston pump and sample flows for aerosols and CO_2. The aerosol sample flow was diluted by particle-free air regulated by a mass flow controller (MFC) to extend the concentration range measured by the UCPC and CPC. The diluted sample flow was then passed through a heated stainless-steel tube (evaporation tube) for heated sampling, or a bypass tube for unheated sampling. The flow was switched between the two paths by an automated three-way valve downstream. The tube downstream of the three-way valve was
575 split into the individual sample flows for the UCPC, CPC, and SMPS. An additional small flow (~0.05 L min–1) was maintained by an orifice, a mass flow meter (MFM), and a pump to avoid the creation of a reverse stream from the evaporation tube during unheated sampling.

https://doi.org/10.5194/acp-2020-395
Preprint. Discussion started: 13 May 2020

Atmospheric Chemistry and Physics Discussions

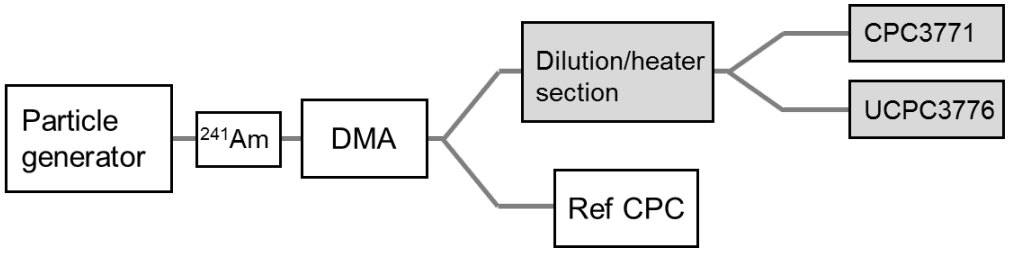

580

Figure 3: Experimental apparatus for the penetration and removal efficiencies experiments. An electrospray aerosol generator (EAG: Model 3480; TSI), a combustion aerosol standard (CAST; Matter Engineering) with a tube furnace for thermal treatment at 350°C, and a custom-made tube furnace for supply of condensable vapours were used to generate polydisperse aerosol particles for the calibrations. 585 Monodisperse aerosol particles were generated by using a bipolar charger conditioner (241Am) and a differential mobility analyzer (DMA). An aerosol electrometer (AE: Model 3068B; TSI) and a reference CPC (ref CPC: Model 3775; TSI) were used as reference instruments.

https://doi.org/10.5194/acp-2020-395
Preprint. Discussion started: 13 May 2020

Atmospheric Chemistry and Physics Discussions

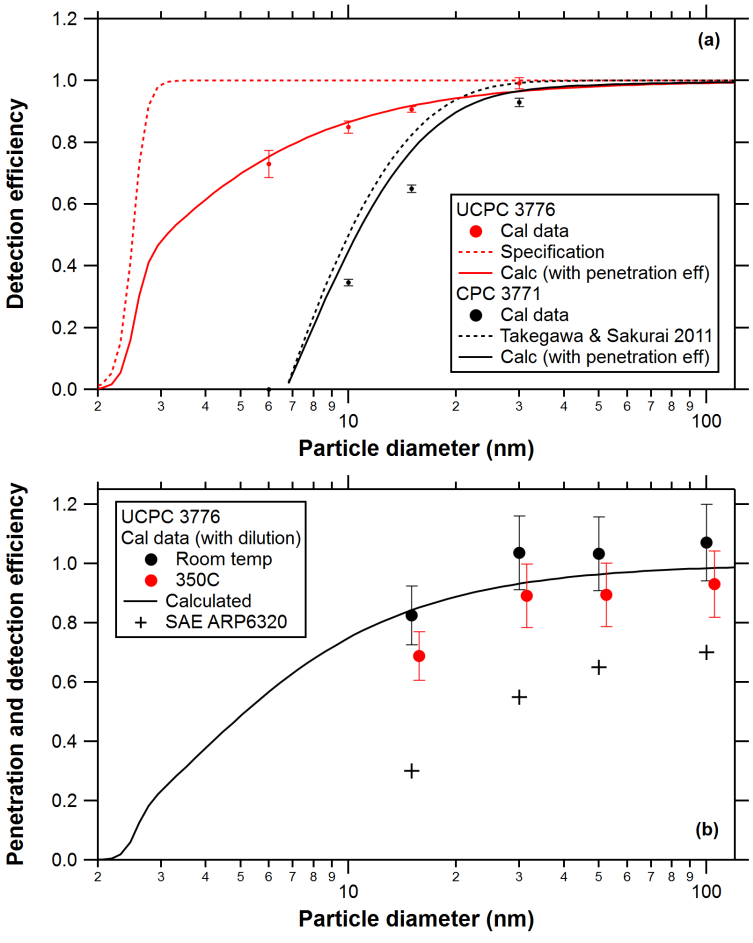

Figure 4: Laboratory evaluation of the performance of the UCPC and CPC. (a) Size-resolved detection efficiencies of the UCPC and CPC measured in the laboratory. (b) Penetration and detection efficiency of non-volatile propane soot particles through the heating-mode sampling tubes at room temperature and at 350°C. The calculated curve includes the penetration efficiency through the dilution/heater section and the detection efficiency of the UCPC at room temperature. The cross symbols represent the minimum penetration efficiency of non-volatile particles specified by the SAE-ARP6320 protocol.

https://doi.org/10.5194/acp-2020-395
Preprint. Discussion started: 13 May 2020

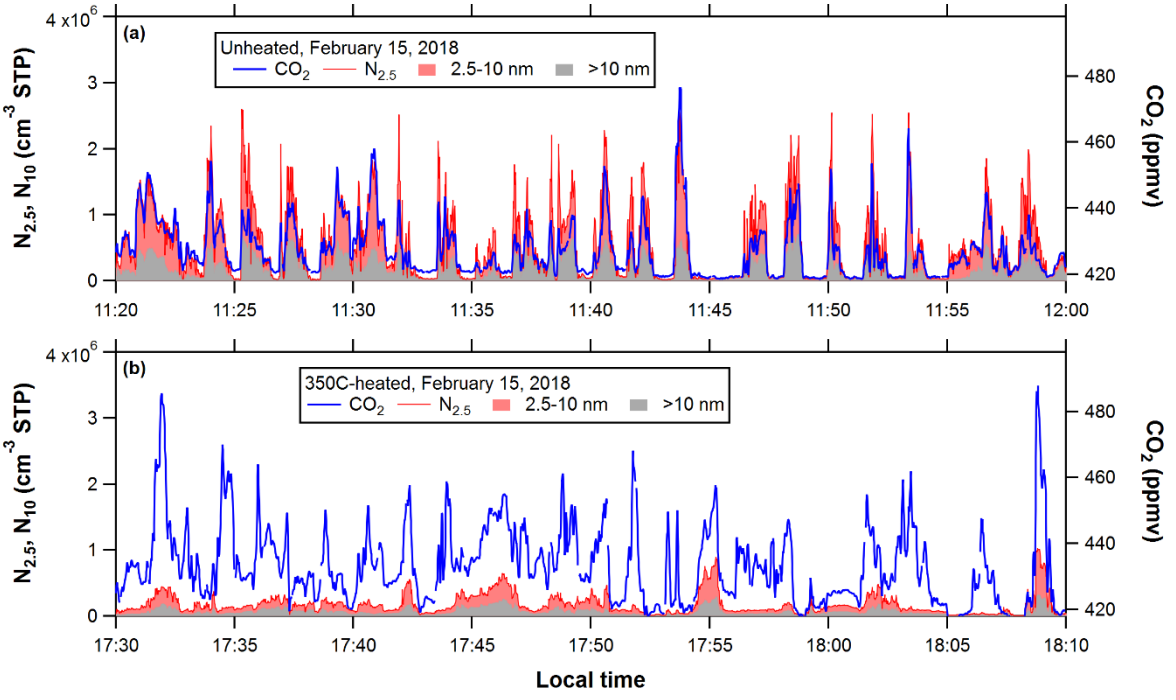

600

Figure 5: Time series of $N_{2.5}$ and CO_2 observed near a runway of NRT. Data for (a) unheated and (b) 350°C-heated modes obtained on February 15, 2018 are shown. The number fractions of particles with diameters ranging from 2.5 to 10 nm (red area) were generally larger than those for particles with diameters above 10 nm (gray area) for both the unheated and 350°C-heated modes.

https://doi.org/10.5194/acp-2020-395
Preprint. Discussion started: 13 May 2020

Atmospheric Chemistry and Physics Discussions

605

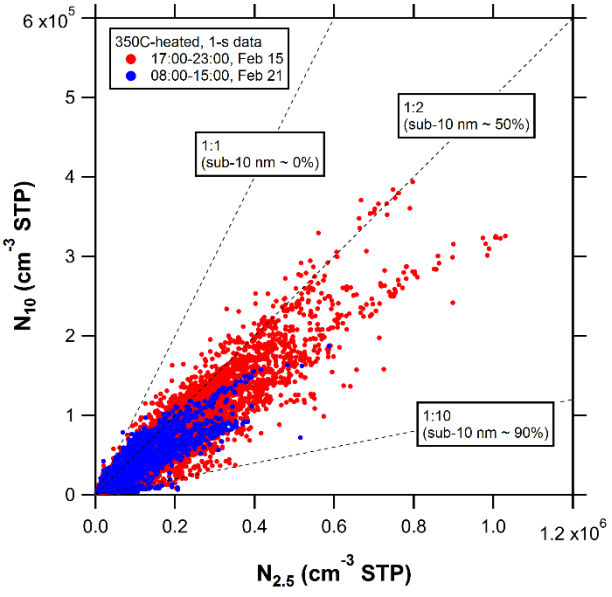

Figure 6: Scatterplots of N_{10} versus $N_{2.5}$ for 350°C-heated mode. Data obtained on February 15, 2018 (red) and February 21, 2018 (blue) are shown. The 1:1 correspondence line ($N_{10} = N_{2.5}$) represents the state in which all particles are included in the size range larger than 10
610 nm.

https://doi.org/10.5194/acp-2020-395
Preprint. Discussion started: 13 May 2020

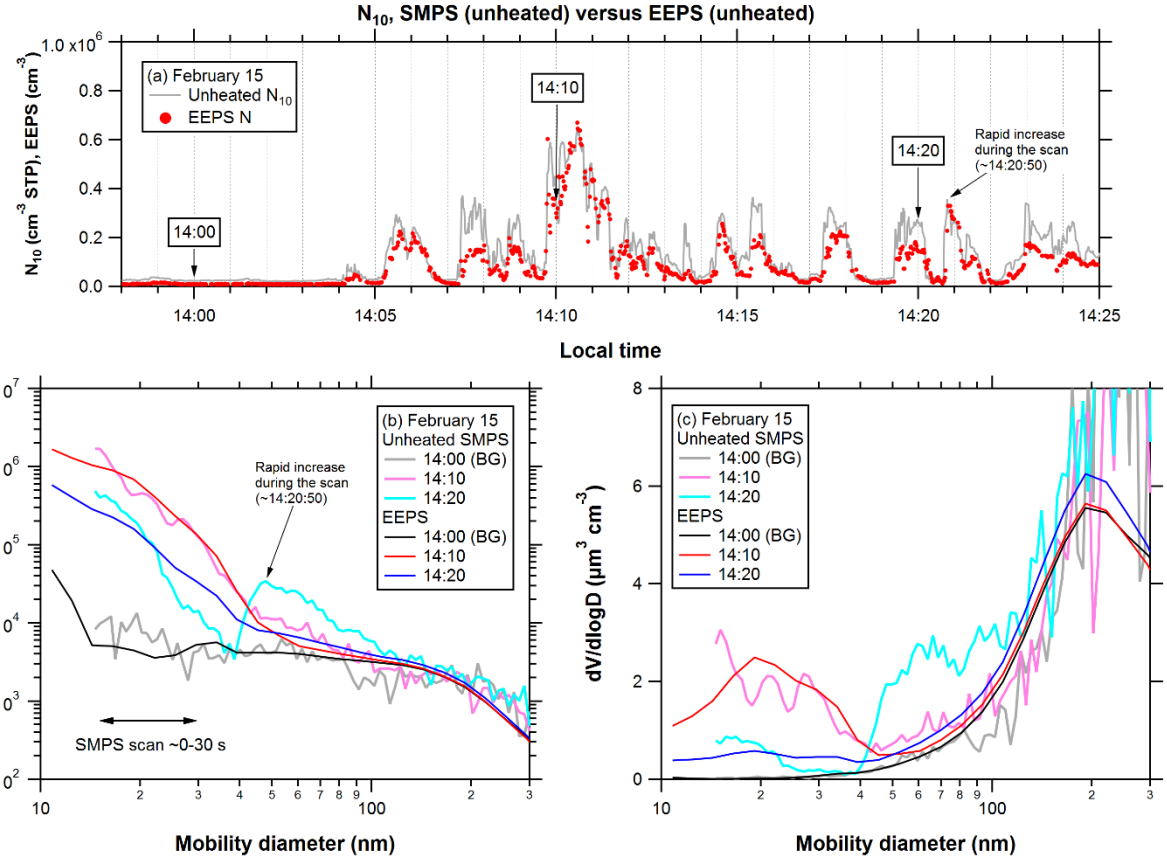

Figure 7: (a) Time series of unheated N_{10} (grey) and total particle number concentrations derived from the EEPS (EEPS N, red) obtained at 13:58-14:25 LT on February 15, 2018. (b) Particle number size distributions as measured simultaneously by the EEPS and unheated SMPS for selected time periods indicated in (a). The EEPS data were averaged over 40 s around the timing of the SMPS scan corresponding to the diameter range of 15–30 nm (i.e., averaged from 10 s before to 30 s after the onset of each SMPS scan). "BG" denotes a time period without enhancements of aerosols and CO_2. (c) Same as (b) but for particle volume size distributions.

https://doi.org/10.5194/acp-2020-395
Preprint. Discussion started: 13 May 2020

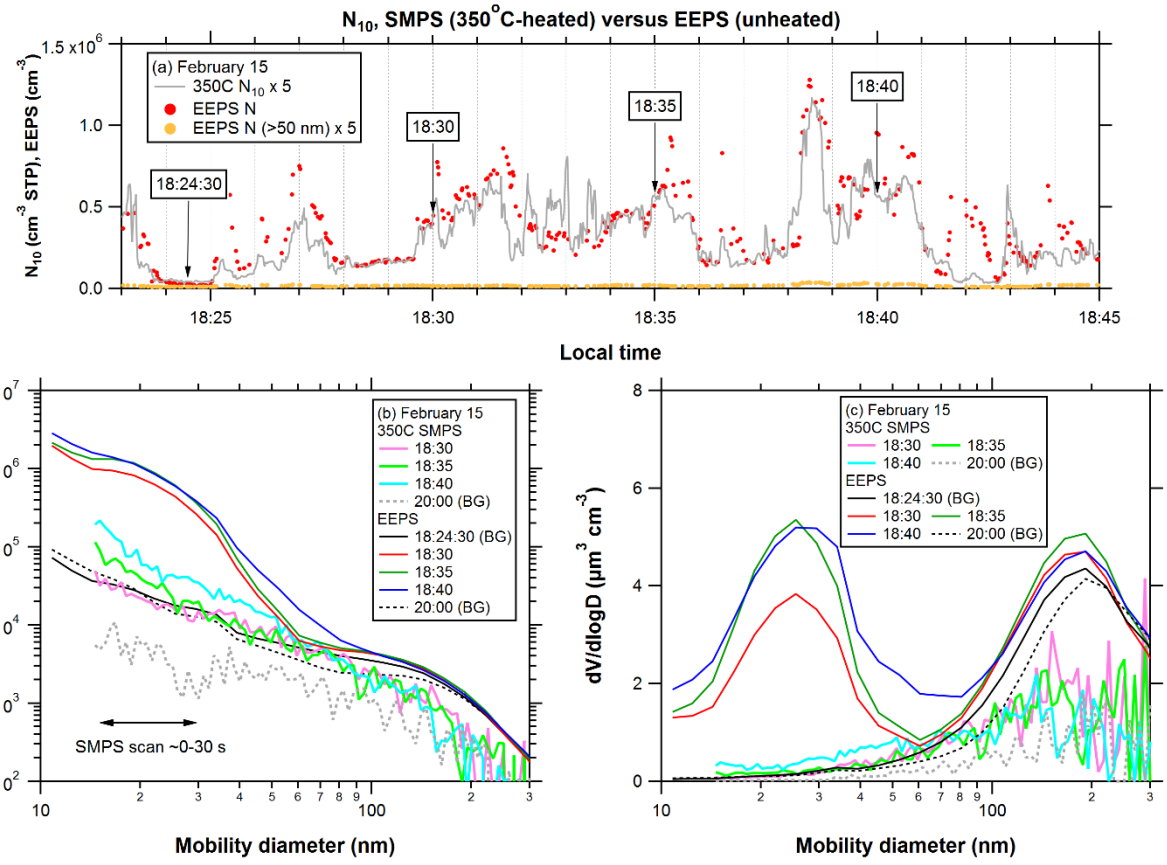

Figure 8: (a) Time series of 350°C-heated N_{10} (grey), total particle number concentrations derived from the EEPS (EEPS N, red), and particle number concentrations for a diameter range of >50 nm measured by the EEPS (EEPS N (>50 nm), orange) obtained at 18:23-18:45 LT on February 15, 2018. The 350°C-heated N_{10} and EEPS N (>50 nm) data are multiplied by a factor of 5 for clarity. (b) Particle number size distributions as measured simultaneously by the EEPS and 350°C-heated SMPS for selected time periods indicated in (a). The average method for the EEPS is the same as that used in Fig. 7b. "BG" denotes a time period without enhancements of aerosols and CO_2. (c) Same as (b) but for particle volume size distributions.

https://doi.org/10.5194/acp-2020-395
Preprint. Discussion started: 13 May 2020

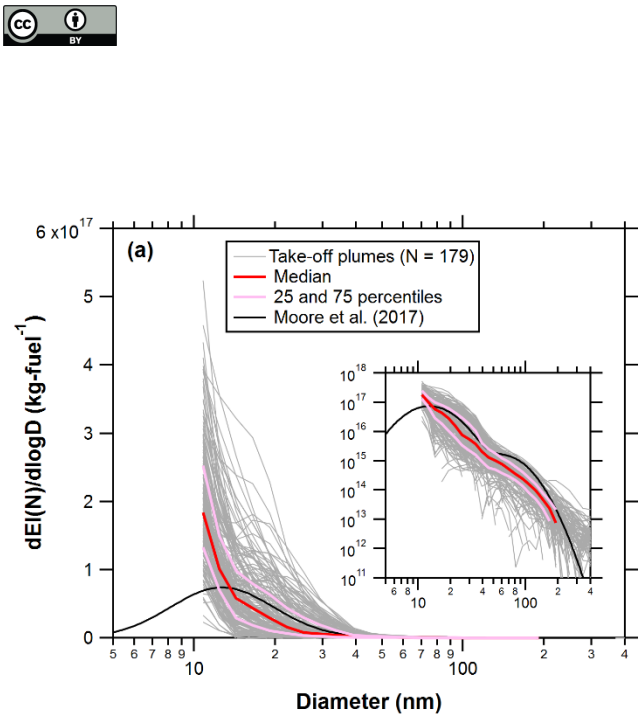

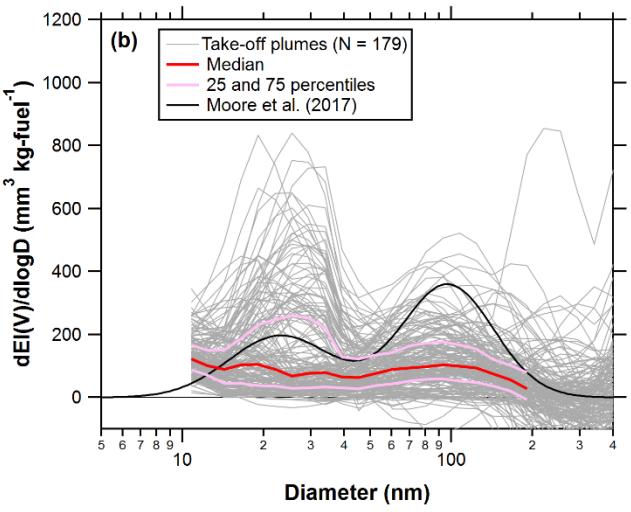

635 **Figure 9:** Size distributions of (a) number and (b) volume EIs derived from the EEPS data for the take-off plumes. The shaded lines represent all data for the take-off plumes. The red and two pink lines indicate the median, 25, and 75 percentiles, respectively. The black line represents the average size distributions from Moore et al. (2017a). A log-log plot of the same data is inserted in (a) for better visualization of smaller values.

https://doi.org/10.5194/acp-2020-395
Preprint. Discussion started: 13 May 2020

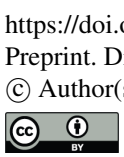

Atmospheric Chemistry and Physics Discussions

640

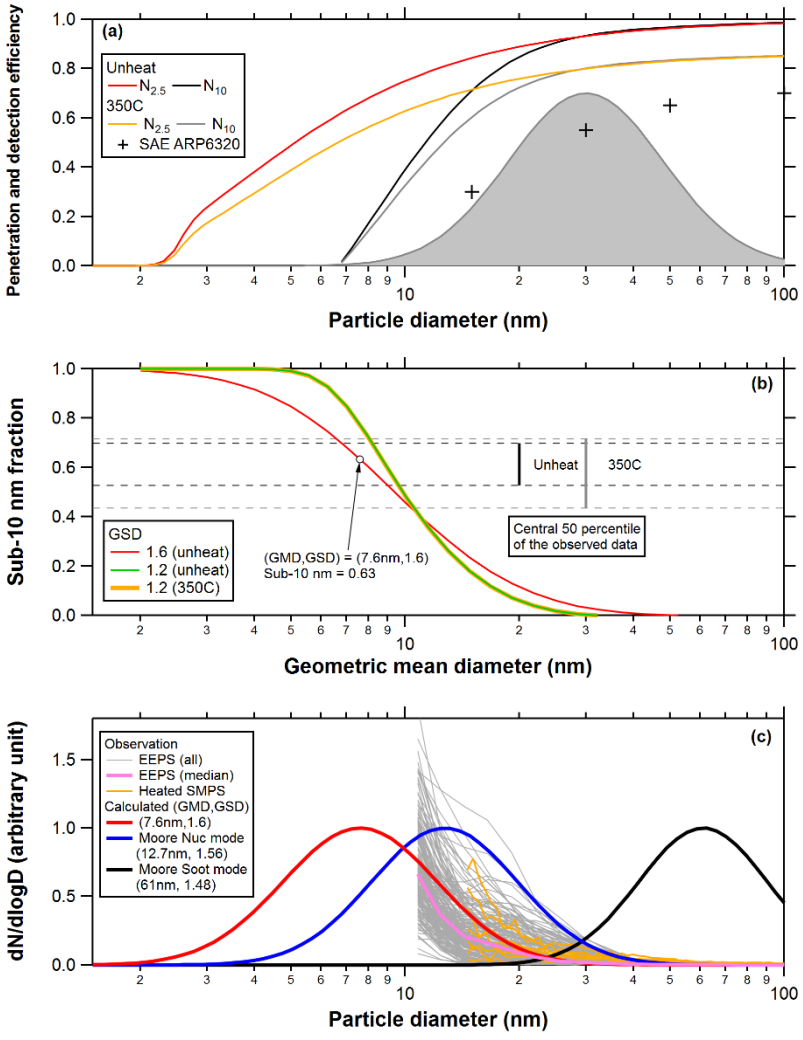

Figure 10: (a) Overall penetration and detection efficiencies for the unheated and 350°C-heated $N_{2.5}$ and N_{10}. The lower limit of the penetration efficiency through the VPR specified in SAE-ARP6320 is shown for comparison. The shaded area represents an example of assumed particle number size distributions for calculating the number fraction of sub-10 nm particles. (b) Number fraction of sub-10 nm particles ($1 - \Delta N_{10}/\Delta N_{2.5}$) obtained by convolution of the penetration and detection efficiency curves in (a) and assumed particle number size distributions having various GMDs and GSDs. The horizontal dashed lines indicate the central 50 percentile range (between 25 and 75 percentiles) of the observed data for the unheated and 350°C-heated mode. The calculation results for the unheated and 350°C-heated modes were nearly identical because we assumed that the size dependency of the penetration efficiency of particles through the evaporation tube for the 350°C-heated mode was the same as that for the unheated mode. (c) An example of the particle number size distributions that can explain the observed median of $\Delta N_{10}/\Delta N_{2.5}$ ratios for the unheated mode (red). The number size distributions with (GMD, GSD) = (12.7 nm, 1.56) and (61 nm, 1.48), which correspond to the average "nucleation mode" and "soot mode" distribution (blue and black, respectively) reported by Moore et al. (2017a), are shown for comparison. The size distributions of particle number EIs for the take-off plumes derived from the EEPS data (Fig. 9a) and particle number size distributions obtained by the 350°C-heated SMPS on February 15, 2018 (Fig. 8b) are also shown.

655

https://doi.org/10.5194/acp-2020-395
Preprint. Discussion started: 13 May 2020

Atmospheric Chemistry and Physics Discussions

Table 1: Particle number emission indices (EIs) (particles kg-fuels^{-1}) and sub-10 nm fractions. The particle number EI values for unheated $N_{2.5}$, unheated N_{10}, 350°C-heated $N_{2.5}$, and 350°C-heated N_{10} are referred to as total EI($N_{2.5}$), total EI(N_{10}), non-volatile EI($N_{2.5}$), and non-volatile EI(N_{10}), respectively.

	25 percentile	50 percentile	75 percentile
Total			
EI($N_{2.5}$)	8.9×10^{16}	1.1×10^{17}	1.3×10^{17}
EI(N_{10})	3.2×10^{16}	4.2×10^{16}	5.2×10^{16}
Sub-10 nm fraction	0.53	0.63	0.70
Non-volatile			
EI($N_{2.5}$)	2.4×10^{15}	5.7×10^{15}	1.1×10^{16}
EI(N_{10})	1.1×10^{15}	1.8×10^{15}	4.0×10^{15}
Sub-10 nm fraction	0.44	0.54	0.72

660